Computers and Structures 165 (2016) 48–58

Contents lists available at ScienceDirect

Computers and Structures

journal homepage: www.elsevier.com/locate/compstruc

A hierarchic high-order Timoshenko beam finite element

C.-Y. Tai [a,b], Y.J. Chan [a,*]

[a] Department of Mechanical Engineering, National Chung-Hsing University, Kuo-Kuang Road, Taichung 40227, Taiwan, ROC
[b] Machine Tools Technology Center, Industrial Technology Research Institute, Wenxian Road, Nantou City 54041, Taiwan, ROC

ARTICLE INFO

Article history:
Received 13 September 2015
Accepted 2 December 2015
Available online 5 January 2016

Keywords:
Timoshenko beam
p-Version finite element method

ABSTRACT

Timoshenko beam theory (TBT) is suitable for vibration studies as it describes beams with small models. The super-convergent Timoshenko beam element is improved by adding hierarchic high-order shape functions using Legendre polynomials, and correction terms were added where necessary. The proposed element is validated in static, dynamic and rotordynamic analyses. With the same model size, the fractional error of the 2nd cantilever beam natural frequency with the *p*-version beam element is 1/100th of the *h*-version counterpart, and error in estimating natural frequency split in rotors is reduced. The proposed element is also applied to estimate natural frequencies in experiments.

1. Introduction

Rotating systems are widely used in power machines. For example, spindle rotor is a key component of a machine tool and its flexural stiffness determines the accuracy of products. Recently, precision and efficiency requirements in manufacturing sector calls for improved spindle rigidity, thus it needs to be thoroughly analysed and managed. A beam model is preferred [7] because its small model size can provide insight of the critical factors affecting performance, and facilitating stochastic studies such as the Monte Carlo Simulation [3].

The Timoshenko beam theory (TBT) [26], which includes the effects of lateral displacement, bending moment, shear deformation and rotary inertia, considers more mechanical phenomena than other popular beam theories [12]. The error of natural frequencies in Timoshenko beam models are also much lower than those formulated using the Euler–Bernoulli beam theory (EBT). Therefore, the TBT is still being used in analysis [7], despite 3-D models being computationally affordable. Majkut [16] has given the natural frequencies of simply-supported and cantilevered Timoshenko beams as solutions of 4×4 matrices, and Horr and Schmidt [13] computed the closed-form solution for a Timoshenko cantilever beam with a range of tip masses.

The Timoshenko beam theory was extensively studied in three fields: (i) the shear correction factor, (ii) existence of the second mode family and (iii) its finite element method implementation:

- The shear correction factor (denoted κ in the discussion below) which depends on the shape of the cross section, is included to address the non-uniform shear stress on a cross section [26,4,23,11,14].
- While two groups of modes exist in Timoshenko beams [25,2], some Timoshenko beam finite elements consider only the low-frequency mode [18]. This is because its existence was challenged [24,18] and Díaz-de-Anda et al. [5] has shown in experiments that the second frequency spectrum can be neglected in evaluating natural frequencies below $\omega^2 = \kappa GA/\rho I$.
- The finite element method is introduced in numerous textbooks such as [27]. Traditional Timoshenko beam elements use linear shape functions for both deflection and rotation, but it can lead to shear locking. Friedman and Kosmatka proposed the interdependent interpolation (also known as "super-convergent") Timoshenko beam element [9,15,21], and improved the two-node Timoshenko beam finite element. The super-convergent beam element is introduced in Section 2 of this work. Although the stiffness matrix formulation of a super-convergent beam element is undisputed, the mass matrix is not [22].

In vibration analysis, mode shapes are usually curved according to sinusoidal and hyperbolic functions, therefore a large number of elements is needed to estimate the first few natural frequencies accurately [20]. This shortcoming can be solved with *p*- or *hp*-version FEM [1], which can reduce the number of degrees of freedom (DOF) and increase computing speed. There are two shape function bases known as the standard and hierarchic basis, and the mass, stiffness and gyroscopic matrices can be formulated once the shape functions are known [10]. Oñate applied standard *p*-version FEM and created 3-noded Timoshenko beam elements to develop

* Corresponding author.
E-mail addresses: harkat_tai@itri.org.tw (C.-Y. Tai), yjchan@nchu.edu.tw (Y.J. Chan).
URL: http://www.me.nchu.edu.tw/ (Y.J. Chan).

http://dx.doi.org/10.1016/j.compstruc.2015.12.002
0045-7949/

quintic shape functions [19], but adopting such high-order shape functions involve recalculation of all matrix entries. Hierarchic shape functions are used to describe Euler–Bernoulli beams [20] and shells [6] with Legendre polynomials, but hierarchic shape functions for Timoshenko beams have not been formulated.

Section 2 of this article outlines the application of Legendre polynomials [1] to model Timoshenko beam finite element. The shape functions are designed to be super-convergent, where the concept was introduced in Ref. [9]. By using high-order shape function, stiffness matrix, mass matrix, axial-load stiffness matrix and gyroscopic matrix are presented in Section 3. In Sections 4 and 5, natural frequencies between low-order and high-order cantilever beam models are compared in numerical demonstration and experiments, respectively. Because the bandwidth of the current analysis is much lower than the critical frequency as discussed in [5], the "second frequency spectrum" and its associated modes is neglected.

2. Theory

2.1. Timoshenko beam theory and super-convergent Timoshenko beam element

The Timoshenko Beam Theory (TBT) is different from the Euler–Bernoulli Beam Theory (EBT) because the EBT enforces the beam cross section to be perpendicular to the centreline of the beam. In the TBT, the angle between the rotation of the centreline and the plane of the cross section is called the shear angle, denoted γ, as shown in Fig. 1:

$$\phi = \frac{dw}{dx} + \gamma \tag{1}$$

The governing equations for a Timoshenko beam are

$$\kappa AG\left(\frac{\partial \phi}{\partial x} + \frac{\partial^2 w}{\partial x^2}\right) - \rho A \frac{\partial^2 w}{\partial t^2} = q \tag{2a}$$

$$\kappa AG\left(\frac{\partial w}{\partial x} + \phi\right) - EI\frac{\partial^2 \phi}{\partial x^2} + \rho I \frac{\partial^2 \phi}{\partial t^2} = 0 \tag{2b}$$

where E, G and ρ are the Young's modulus, shear modulus and material density, respectively. Geometric parameters in Eq. (4) include moment of inertia I, cross sectional area A and the shear correction factor κ. The shear coefficient expressions formulated by Hutchinson [14] are adopted in this work. Shear coefficient for selected cross sections are given in Eq. (3):

$$\kappa = \frac{6(1+\nu)^2}{7+12\nu+4\nu^2} \qquad \text{Solid shafts} \tag{3a}$$

$$\kappa = \frac{6(r_i^2+r_o^2)(1+\nu)^2}{20r_i^2r_o^2+(7+12\nu+4\nu^2)(r_i^2+r_o^2)^2} \qquad \text{Hollow shafts} \tag{3b}$$

$$\kappa = -\frac{2(1+\nu)}{\frac{9C}{4h^3b}+\nu\left(1-\frac{b^2}{h^2}\right)} \qquad \text{Rectangular beam} \tag{3c}$$

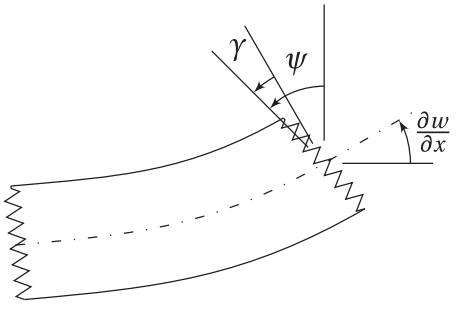

Fig. 1. Shear angle in Timoshenko beam model.

where r_i is the inner radius, r_o is outer radius, ν is the Poisson ratio, $2b$ is the width of the beam, $2h$ the height of the beam and

$$C = \frac{4}{45}h^3b\left(-12h^2+15\nu h^2+5\nu b^2\right) + \sum_{n=1}^{\infty}\frac{16\nu^2b^5\left(n\pi h - b\tanh\left(\frac{n\pi h}{b}\right)\right)}{(n\pi)^2(1+\nu)}$$

Assuming separation of variables (that is, $w(x,t) = W(x)T(t)$ and $\phi(x,t) = P(x)T(t)$) Eq. (2) becomes Eq. (4):

$$\kappa AG\frac{\partial}{\partial x}\left(\frac{\partial w}{\partial x}+\phi\right) = q(x,t) \tag{4a}$$

$$\kappa AG\left(\frac{\partial w}{\partial x}+\phi\right) - EI\frac{\partial^2\phi}{\partial x^2} = 0 \tag{4b}$$

In traditional finite element formulation, there were difficulties in forming shape functions to fulfill Eq. (2). In this case, shear locking occurs and the deflection computed using the finite element method would be much lower than the true solution.

Shear locking is avoided in super-convergent Timoshenko beam elements [9,15] because each displacement shape function corresponds to a rotation shape function. There are four displacement shape functions in a super-convergent beam element. In constructing super-convergent Timoshenko beam elements, the shape functions for rotation are first derived, and the corresponding shape for deflection for each rotation shape is sought using Eq. (4). As a result, the pairs of deflection and rotation shapes always satisfy the constitutive equations. Such formulation does not determine the pure shear frequency $\omega^2 = \kappa GA/\rho I$ but it is shown to achieve good results at low frequencies [9,22].

If the right hand side of Eq. (4a) is enforced to be zero as in typical EBT finite element, the shear angle in an element can be assumed to be constant [9], rotation and deflection shape functions are found to be quadratic and cubic, respectively. The four basic rotation shape functions for a super-convergent Timoshenko beam element, in isoparametric coordinate ξ, are shown in Eq. (6) [9]:

$$[N_\phi] = \frac{1}{1+12\Omega}\begin{Bmatrix} \frac{3}{2L}(\xi^2-1) \\ \frac{1}{4}(3\xi^2-2(1+12\Omega)\xi-1+24\Omega) \\ -\frac{3}{2L}(\xi^2-1) \\ \frac{1}{4}(3\xi^2+2(1+12\Omega)\xi-1+24\Omega) \end{Bmatrix} \tag{5}$$

where

$$\xi = \frac{2x}{L}-1, \quad \frac{d\xi}{dx} = \frac{2}{L}, \quad \Omega = \frac{EI}{\kappa GAL^2}$$

and the displacement vector being

$$q = \{\, w_1 \quad \phi_1 \quad w_2 \quad \phi_2 \,\}^T$$

Correspondingly, the deflection shape functions can be sought by combining Eq. (5) and (4b):

$$[N_w] = \frac{1}{1+12\Omega}\begin{Bmatrix} \frac{1}{4}(\xi^3-(3+24\Omega)\xi+2(1+12\Omega)) \\ -\frac{L}{8}(-\xi^3+(1+12\Omega)\xi^2+\xi-(1+12\Omega)) \\ -\frac{1}{4}(\xi^3-(3+24\Omega)\xi-2(1+12\Omega)) \\ \frac{L}{8}(-\xi^3+(1+12\Omega)\xi^2-\xi-(1+12\Omega)) \end{Bmatrix} \tag{6}$$

The shape functions in Eq. (6) and (5) are called "nodal modes" in subsequent discussion, as each of them implies deflection at one specific nodal degree of freedom.

2.2. High-order shape functions and Legendre polynomials

It is known that the results of *p*-version EBT finite elements are more accurate than those of the *h*-version counterpart [17,19]. While *p*-version Euler–Bernoulli beam element has been established with Legendre polynomials, various options of *p*-version of Timoshenko beams have been attempted, such as the three-node *p*-version Timoshenko beam [19]. However, the hierarchic *p*-version Timoshenko beam is more attractive because of the embedding property, which states that the system matrices for a lower-order beam element is always a sub-matrix of the system matrices with a higher order [17].

Legendre polynomials are chosen to build shape functions. The *n*th Legendre polynomial is determined by the Rodriguez formula [20]:

$$\mathcal{L}_m(\xi) = \frac{1}{m!(-2)^m}\frac{d^m}{d\xi^m}\left[\left(1-\xi^2\right)^m\right] \tag{7}$$

The first four Legendre polynomials are listed in Eq. (8) for convenience:

$$\mathcal{L}_0(\xi) = 1 \tag{8a}$$
$$\mathcal{L}_1(\xi) = \xi \tag{8b}$$
$$\mathcal{L}_2(\xi) = \frac{3}{2}\xi^2 - \frac{1}{2} \tag{8c}$$
$$\mathcal{L}_3(\xi) = \frac{5}{2}\xi^3 - \frac{3}{2}\xi \tag{8d}$$

It is noted that $\mathcal{L}_i(\xi)$ is an odd function if i is odd, and $\mathcal{L}_i(\xi)$ is an even function if i is even. Any two Legendre polynomials $\mathcal{L}_n$ and $\mathcal{L}_m$ are orthogonal to each other (Eq. (9)):

$$\int_{-1}^{1}\mathcal{L}_n(\xi)\mathcal{L}_m(\xi)d\xi = \begin{cases}\frac{2}{2n+1} & \text{if } n=m\\ 0 & \text{otherwise}\end{cases} \tag{9}$$

As each super-convergent Timoshenko beam element has four DOFs, the first high-order shape function becomes the 5th shape function, the second high-order shape function becomes the 6th, and so on. To pick a suitable way of constructing high-order shape functions, the limit of slender beam is considered. In a slender beam, the strain energy is dominated by the bending term:

$$U \approx \frac{1}{2}\int_0^L \phi(x)'EI\phi'(x)dx = \frac{1}{2}\int_0^L \sum_i\sum_j \alpha_{ij}N'_{i\phi}(x)EIN'_{j\phi}(x)dx \tag{10}$$

If the derivatives of the rotation shape functions are orthogonal to each other, the high-order part of the stiffness matrix would be diagonal. The construction of odd- and even-order high-order shape functions are introduced separately, with the 5th and 6th shape functions demonstrated as examples.

2.2.1. Odd-order shape functions

To satisfy Eq. (10), the odd-order shape functions are constructed according to Eq. (11):

$$N_{i\phi}(\xi) = \frac{1}{(1+12\Omega)L}\sqrt{\frac{2i-5}{2}}\int_{-1}^{\xi}\mathcal{L}_{i-3}(\varsigma)d\varsigma \tag{11}$$

Such an arrangement has an additional advantage that the shape functions become zero at the nodes (such a property means those shape functions are also known as "bubble shapes"). The orthogonal property of Legendre polynomials implies

$$\int_{-1}^{1}\frac{dN_{i\phi}}{d\xi}\frac{dN_{j\phi}}{d\xi}d\xi = \frac{1}{L^2(1+12\Omega)^2}\delta_{ij} \tag{12}$$

for $i = 5, 7, \ldots$ and j being any positive integer. After $N_{i\phi}(\xi)$ is sought, $N'_{iw}(\xi)$ is evaluated using Eq. (4b) as

$$\kappa AG\left(\frac{2}{L}\frac{\partial N_{iw}(\xi)}{\partial\xi} + N_{i\phi}(\xi)\right) - \frac{2EI}{L^2}\frac{\partial^2 N_{i\phi}(\xi)}{\partial\xi^2} = 0$$

The deflection shape function $N_{iw}(\xi)$ can be sought by integration, with additional constraints of $N_{iw}(\pm1) = 0$ is applied to maintain the "bubble mode shapes":

$$N_{iw}(x) = \int_0^x N'_{iw}(\varsigma)d\varsigma$$
$$N_{iw}(\xi) = \frac{L}{2}\int_{-1}^{\xi}N'_{iw}(\varsigma)d\varsigma$$

To demonstrate the procedure, the 5th rotation and deflection shape functions are derived below. According to Eq. (11),

$$N_{5\phi}(\xi) = \frac{1}{(1+12\Omega)L}\frac{\sqrt{10}}{2}\int_{-1}^{\xi}\mathcal{L}_2(\varsigma)d\varsigma$$
$$= \frac{1}{(1+12\Omega)L}\frac{\sqrt{10}}{4}\left[\varsigma^3-\varsigma\right]_{-1}^{\xi} = \frac{1}{L(1+12\Omega)}\frac{\sqrt{10}}{4}\left(\xi^2-1\right)\xi \tag{13}$$

As the deflection shape function is related to the rotation shape function by Eq. (4b):

$$N'_{5w}(\xi) = \Omega L^2 N''_{5\phi} - N_{5\phi} = \frac{\sqrt{10}}{(1+12\Omega)}\left(\frac{6\Omega}{L}\xi - \frac{1}{4L}\left(\xi^3-\xi\right)\right)$$

therefore

$$N_{5w}(\xi) = \frac{\sqrt{10}}{2(1+12\Omega)}\left(-\frac{1}{16}\xi^4 + \left(\frac{1}{8}+3\Omega\right)\xi^2 - \left(\frac{1}{16}+3\Omega\right)\right) \tag{14}$$

Referring to Eq. (4a), the distribution of the shear angle associated with this shape function is found to be linear:

$$N_{5\gamma} = N_{5\phi} + N'_{5w} = \frac{6\sqrt{10}\Omega}{(1+12\Omega)L}\xi$$

2.2.2. Even-order shape functions and correction term

The same approach shown above can be applied to even-order high-order shape functions with a minor modification, which is necessary due to the number of constraints. The 6th shape function is taken to support the arguments. As $N_{5\phi}$ is a cubic and odd polynomial, $N_{6\phi}$ is assumed to be quartic and even (Eq. (15)):

$$N_{6\phi}(\xi) = p_4\xi^4 + p_2\xi^2 + p_0 \tag{15}$$

which leads to its second derivative and $N_{6w}(\xi)$ being quadratic and quintic, respectively:

$$N''_{6\phi}(\xi) = \frac{48p_4}{L^2}\xi^2 + \frac{8p_2}{L^2}, \qquad N_{6w}(\xi) = r_5\xi^5 + r_3\xi^3 + r_1\xi$$

There are totally 6 variables in $N_{6\phi}$ and N_{6w} bound by the following constraints:

1. Coefficients p_4, p_2 and p_0 would be fixed if $N_{6\phi}(\xi)$ were derived directly from Eq. (11).
2. Three constraints are introduced by Eq. (16), which is based on Eq. (4b). Coefficient for each term in the polynomial should be equal to zero.

$$\kappa AG\left(\frac{10r_5}{L}\xi^4 + \frac{6r_3}{L}\xi^2 + \frac{2r_1}{L} + p_4\xi^4 + p_2\xi^2 + p_0\right) - EI\left(\frac{48p_4}{L^2}\xi^2 + \frac{8p_2}{L^2}\right) = 0 \tag{16}$$

3. An additional constraint is imposed by boundary condition $N_{6w}(\pm1) = 0$.

Therefore, the number of constraints to be fulfilled is more than the number of coefficients, thus only the trivial solution satisfy all the requirements. The number of coefficients and constraints in selected shape functions are listed in Table 1.

The proposed solution to this problem is to introduce an additional coefficient (or a "correction term") to $N_{i\phi}$ for even-order i, such that the number of coefficients and constraints are equal. Such a coefficient should accompany an even function, and a natural choice is $\int \mathcal{L}_1 d\xi$ as it can adjust the shape function without introducing rotation at nodes. Therefore, the high-order shape function is sought using Eq. (17) if i is even:

$$N_{i\phi}(\xi) = \frac{1}{(1+12\Omega)L}\sqrt{\frac{2i-5}{2}}\int_{-1}^{\xi}(\mathcal{L}_{i-3}(\varsigma)+s_i\varsigma)d\varsigma \tag{17}$$

and the rest of the procedure is the same as the odd-order shape functions. For example, the 6th shape function for rotation is defined from Legendre polynomials and the correction term:

$$N_{6\phi} = \frac{\sqrt{14}}{16L(1+12\Omega)}(5\xi^4 - 6\xi^2 + 1) + s_6(\xi^2 - 1)$$

The deflection shape function is, as before, sought using Eq. (4b) and the given boundary conditions. It can be determined that the correction factor s_6 is equal to

$$s_6 = -\frac{3\Omega\sqrt{14}}{(12\Omega+1)^2 L}$$

thus the rotation and displacement shape functions can be obtained:

$$N_{6\phi}(\xi) = \frac{\sqrt{14}}{16L(12\Omega+1)}\left(5\xi^4 - 6(1+8\Omega)\xi^2 + (1+48\Omega)\right) \tag{18a}$$

$$N_{6w}(\xi) = \frac{-\sqrt{14}\xi}{32(1+12\Omega)}\left(\xi^4 - \frac{2(480\Omega^2+60\Omega+1)}{1+12\Omega}\xi^2 + \frac{960\Omega^2+108\Omega+1}{1+12\Omega}\right) \tag{18b}$$

The 5th and 6th displacement and rotation shape functions are shown in Fig. 3 under various values of Ω. For a slender beam where $\Omega \to 0$, the shape of the rotation and displacement shape functions can be determined by integrating the Legendre polynomials once and twice, respectively [20]. The first 7 displacement and rotation shape functions are listed in Appendix A.

3. System matrices

For dynamic analysis of rotating shafts, geometric stiffness due to axial load and gyroscopic effect have to be considered. Therefore, the following equation of motion has to be solved to find natural frequencies, mode shapes and rotor stiffness upon rotation:

$$[M]\{\ddot{q}\} + \Omega_r[G]\{\dot{q}\} + ([K] + [K_f])\{q\} = 0 \tag{19}$$

where Ω_r is the rotating speed of the shaft. $[M]$, $[G]$, $[K]$ and $[K_f]$ refer to the mass matrix, gyroscopic matrix, stiffness matrix and the geometric stiffness matrix, respectively, and are collectively known as "system matrices". The procedure to derive system matrices of a high-order Timoshenko beam element are shown in this section.

Table 1
Number of coefficients and constraints in shape functions before correction.

Shape functions	Coefficients			Constraints			
	N_w	N_ϕ	Total	Legendre	Eq. (4b)	B.C.	Total
1–4	4	3	7	0	3	4	7
5	3	2	5	2	2	1	5
6	3	3	6	3	3	1	7
7	4	3	7	3	3	1	7
8	4	4	8	4	4	1	9

The generalised displacement vector $\{q\}$ includes all degrees of freedom in a beam element. In a planar beam on x–z plane, the degrees of freedom are arranged such that

$$q = \{\, w_1 \quad \phi_1 \quad w_2 \quad \phi_2 \quad w_{5xz} \quad w_{6xz} \,\}^T$$

where w_{5xz} and w_{6xz} are coefficients referred to the high-order shape functions. The nodal degrees of freedom are annotated in Fig. 2.

For the ease of application, system matrices of a Timoshenko beam element with 2 high-order shape functions are listed in Appendix B.

3.1. Mass and stiffness matrices

Considering a two dimension beam (in Fig. 4), the finite element presentation of the equations of motion which is developed by substituting the displacement distribution into Hamilton's principle is [9]

$$[M]\{\ddot{q}\} + [K]\{q\} = 0$$

The mass and stiffness matrices are constructed by considering the kinetic and strain energies in a beam element, respectively. Largely following the approach shown in [9], the mass and stiffness matrices are given by Eq. (20):

$$[M] = \int_0^L \left([N_w]^T \rho A [N_w] + [N_\phi]^T \rho I [N_\phi]\right) dx \tag{20a}$$

$$[K] = \int_0^L \left(\frac{\partial}{\partial x}[N_\phi]^T EI \frac{\partial}{\partial x}[N_\phi] + [N_\gamma]^T \kappa GA [N_\gamma]\right) dx \tag{20b}$$

where $[N_w]$, $[N_\phi]$ and $[N_\gamma]$ are collections of deflection, rotation and shear strain shape functions, respectively. The shear strain shape functions are directly calculated using the deflection and rotation shapes:

$$[N_\gamma] = [N_\phi] + \frac{\partial}{\partial x}[N_w]$$

The two parts in each equation in Eq. (20) can be integrated separately but both terms depend on flexural rigidity EI due to the definition of Ω (Eq. (5)). Also, the "Legendre" and "correction term" can be integrated separately in calculating the stiffness matrix as well.

3.2. Geometric stiffness matrix

Beams and shafts often experience axial loads. The couple formed by the offset axial forces has a stiffening effect if the beam is in tension or a softening effect if the force is compressive (Fig. 4). Considering the work done of the couple, the strain energy related to axial tension f_e can be written [10]:

$$U_f = \frac{f_e}{2}\int_0^l \left(\frac{\partial w(x,t)}{\partial x}\right)^2 dx$$

The geometric stiffness matrix can be built if the shape functions are known [10]:

$$[K]_f = f_e \int_0^l \left[\frac{\partial}{\partial x}[N_w]\right]^T \left[\frac{\partial}{\partial x}[N_w]\right] dx \tag{21}$$

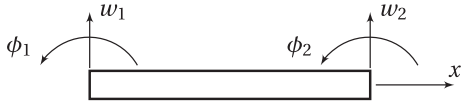

Fig. 2. Notation of deflection and rotation on one plane.

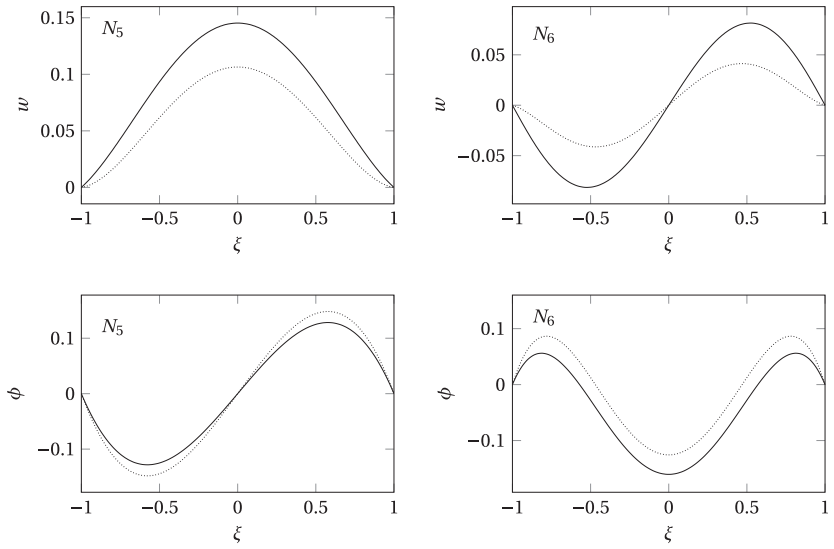

Fig. 3. The 5th and 6th deflection (upper) and rotation (lower) shape functions in isoparametric coordinates. (solid line: $\Omega = 0.0155$, dotted line: $\Omega = 0.0022$.)

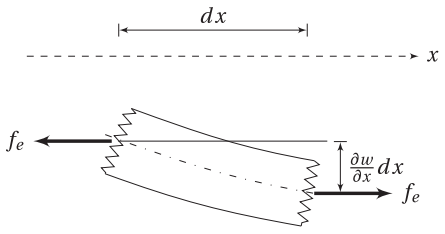

Fig. 4. Effect of axial load on beam segment.

The geometric stiffness matrix of a Timoshenko beam with high-order shape functions is shown in Appendix B.

3.3. Gyroscopic matrix

Gyroscopic effect is evident in rotating structures and leads to mode splitting in cyclic-symmetric structures upon rotation. The local coordinates in the two bending planes are annotated in Fig. 5 [10], and degrees of freedom of the element are described by

$$\{q\} = \{w_1 \quad v_1 \quad \phi_1 \quad \theta_1 \quad w_2 \quad v_2 \quad \phi_2 \quad \theta_2 \quad w_{5xz} \quad w_{5xy} \quad w_{6xz} \quad w_{6xy}\}^T$$

where w_{ixz} and w_{ixy} with $i \geqslant 5$ are degrees of freedom related to high-order shape functions on the x–z and the x–y planes, respectively. The kinetic energy related to gyroscopic effects is

$$T_G = -2\rho I \Omega_r \int_0^L \dot{\phi}(x,t)\theta(x,t)d\xi$$

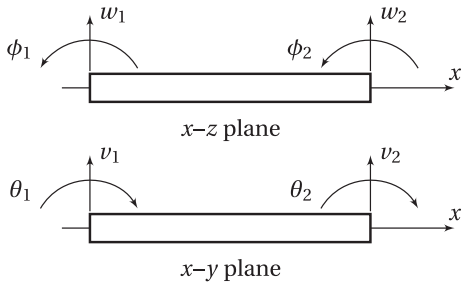

Fig. 5. Notation of deflection and rotation in the two bending planes (adapted from [10]).

The rotations θ_i and ϕ_i are the rotation of Node i on the two planes, which can be expressed in terms of the shape functions:

$$\begin{Bmatrix} \theta_i \\ \phi_i \end{Bmatrix} = \begin{bmatrix} 0 & -N'_{1w} & N'_{2w} & 0 & 0 & -N'_{3w} & N'_{4w} & 0 & 0 & -N'_{5w} & 0 & -N'_{6w} \\ N'_{1w} & 0 & 0 & N'_{2w} & N'_{3w} & 0 & 0 & N'_{4w} & N'_{5w} & 0 & N'_{6w} & 0 \end{bmatrix} \{q\} = [B]\{q\} \tag{22}$$

where $[B]$ is the strain–displacement matrix. The gyroscopic matrix is derived with the help of Lagrange equation [10] with the individual entries determined using Eq. (23):

$$G_{ij} = -\rho I \int_0^L (B_{2i}B_{1j} - B_{2j}B_{1i})dx \tag{23}$$

The gyroscopic matrix is skew-symmetric, as shown in Appendix B.

4. Numerical demonstration

The accuracy and efficiency of the proposed p-version Timoshenko beam finite element are validated using two cantilever beam models in static, vibration and rotordynamics problems as shown below.

4.1. Static analysis

A cantilever beam with rectangular cross section is taken for static analysis. The advantage of the h-version super-convergent beam finite element over other models has been shown in previous research [9], and this work is focused on comparing the results from the h- and p-version FE results. The beam is made of aluminium and properties of the model are shown in Table 2, and the shear coefficient is equal to $\kappa = 0.8963$ according to Eq. (3c). The models with different numbers of bubble shape functions have roughly the same number of DOFs for a reasonable comparison.

A uniformly-distributed lateral load of q_0 is applied to the cantilever beam as an example. In such a case, the tip displacement w_t, the bending moment at the fixed end M_b and the shear force at the fixed end Q_b can be expressed analytically [9]:

$$w_t = \frac{q_0 L^4}{8EI}(1 + 4\Omega), \quad M_b = \frac{q_0}{2}L^2, \quad Q_b = q_0 L \tag{24}$$

In the finite element computations, the bending moment and shear force can be evaluated using the displacement profile:

$$M(x) = EI\frac{d\theta}{dx}, \quad Q(x) = kGA\left(\frac{dw}{dx} + \theta\right) \tag{25}$$

Basic EBT has demonstrated that the deflection, bending moment and shear force profiles of a uniformly-loaded cantilever beam are quartic, quadratic and linear polynomials, respectively. Because the basic shape functions of a super-convergent Timoshenko beam element are cubic, the finite element results are not exact. In theory, with an additional bubble shape function added to each element, the stress and displacement profiles can be exactly represented. The meshes listed in Table 3 have the same number of DOFs in the system, except the model with 200 low-order elements which is taken for reference. The results shown in Table 3 show that while the tip deflection between the *h*- and *p*-version finite element methods are virtually the same, the error of shear force at the fixed end in a static analysis can be as high as 8.3% using as many as 6 elements. This error can be eliminated if the DOFs are used to represent high-order terms, without increasing the total number of DOFs.

4.2. Natural frequencies and mode shapes

The first six natural frequencies are used to evaluate the efficiency and accuracy of hierarchic *p*-version FEM over the *h*-version counterpart. The "analytical" natural frequencies of a Timoshenko cantilever (ω_t) are sought using interpolation of matrix determinant [16]. It is noted that the analytical mode shapes of a cantilever involve trigonometric and hyperbolic functions [16], which can be expressed as polynomials with an infinite number of terms. In *h*-version finite element, the infinite polynomials representing the displacement mode shapes are approximated piecewise with cubic polynomials. With high-order shape functions, a closer fit of mode shape is expected, reducing the error in natural frequency.

It is known that the natural frequencies sought from the finite beam models converge to values different from the analytical counterpart due to method of integration [15], therefore, the natural frequencies of high-order models are compared with a super-convergent finite element Timoshenko beam model with 2000 elements, denoted ω_b. The error in natural frequencies listed in Table 4 (and plotted in Fig. 6) show that, the natural frequency error is reduced by shifting the finite element model from *h*-version to *p*-version, with the same number of DOFs. In particular, the error in 2nd and 3rd natural frequencies are reduced by an order of two by taking 3 high-order shape functions per element. From another viewpoint, for any specified threshold of acceptance, high-order models leads to more natural frequencies being acceptable than the low-order one. Natural frequency calculations are repeated for beams experiencing axial tension $P = 0.5P_{cr}$ (P_{cr} being the Euler buckling load) and the results shown in Fig. 7 shows similar trends in error level. Based on these results, a similar trend on estimating natural frequencies of beams on other boundary conditions are expected.

The mode shape error on cantilevered beams without load between *h*-version and *p*-version finite element models were compared in terms of strain energy. The derivative of the strain energy (U) is found to be proportional to $(\partial\phi/\partial x)^2$ (Eq. 10), and the discrepancy between a given model and the 2000-element counterpart. By shifting the calculation effort from mesh refinement to additional shape functions, the error in strain energy along the beam is decreased by approximately an order of two (Fig. 8). Also, the error is shown to be monotonically decreasing if the number of DOFs remains constant (Fig. 9), probably due to the high-order polynomials giving a closer fit to the mode shape, which is a polynomial with an infinite number of terms.

Table 2
Properties of beam model.

Material properties			Geometric properties		
Young's modulus	E	69 GPa	Height	$2h$	0.02 m
Poisson ratio	ν	0.33	Width	$2b$	0.03 m
Density	ρ	2708.79 kg/m^3	Length	L	0.8 m

Table 3
Error of selected parameters in cantilever beam deflection using *h*- and *p*-version FEM.

High-order shapes/element	0	0	1	2
Elements	200	6	4	3
DOF in the system	400	12	12	12
w_t/w_{t0}	$< 10^{-9}$	$< 10^{-9}$	$< 10^{-9}$	$< 10^{-9}$
M_b/M_{b0}	-4.2×10^{-6}	-0.0046	0	0
Q_b/Q_{b0}	-0.0025	-0.0833	0	0

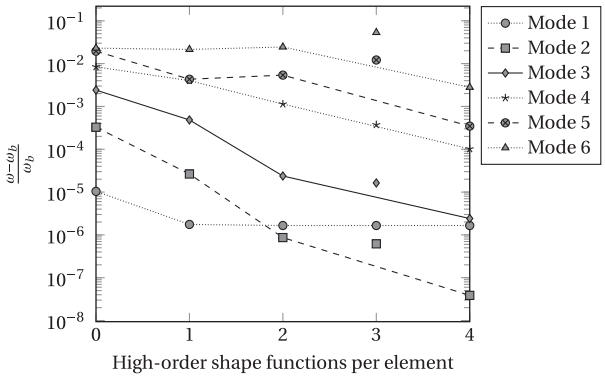

Fig. 6. Error of first six natural frequencies using *h*- and *p*-version FEM. Note: model with $p = 3$ involves 10 DOFs while the others involve 12.

4.3. Rotordynamic analysis

The repeated natural frequencies of rotors are split when double-symmetric rotors rotate, due to gyroscopic forces [10]. The extent of frequency split under *h*- and *p*-version Timoshenko beam element under rotation is evaluated with the model sketched in Fig. 10 with the parameters shown. One end of circular steel rod is "fixed" in one end to resemble a fixed end of a cantilever beam (while it is allowed to rotate along the axis of the shaft), and a disk is attached to the free end. A section near to the free end is modelled as a single low-order element, with the rest of the shaft is modelled using 12 low-order elements or with *p*-version finite elements leading to the same amount of DOFs. The rotation speed is set at $\Omega_r = 1000$ rad/s or 9549 rpm.

The first four mode shapes are sketched in Fig. 11, and the fractional natural frequency split are shown in Fig. 12. A set of baseline results is calculated using a model with 200 low-order finite elements. Firstly, although the error of the first four natural frequencies without rotation are small, more elements are needed to achieve satisfactory accuracy in determining the split natural frequencies, hence 52DOFs are used to model a rotating shaft, compared with 12 DOFs (that is, 24 DOFs on two planes) used in natural frequency analysis. Also, the results in Fig. 12 shows that the extent of natural frequency split is better estimated using *p*-version beam elements, if the amount of DOFs is restricted.

5. Experimental validation

Besides numerical demonstration, the natural frequencies and mode shapes obtained from the high-order Timoshenko beam

Table 4
Fractional error of first six natural frequencies of cantilever beam using *h*- and *p*-version FEM.

Bubble shapes per element			0	1	2	3	4
Elements			6	4	3	2	2
DOFs in system			12	12	12	10	12
Mode	ω_t (Hz)	ω_b (Hz)			$\frac{\omega-\omega_b}{\omega_b}$		
1	25.49	25.47	1.04×10^{-5}	1.76×10^{-6}	1.66×10^{-6}	1.66×10^{-6}	1.66×10^{-6}
2	159.7	159.1	3.28×10^{-4}	2.64×10^{-5}	8.66×10^{-7}	6.18×10^{-7}	3.87×10^{-8}
3	446.1	443.6	2.41×10^{-3}	4.84×10^{-4}	2.37×10^{-5}	1.63×10^{-5}	2.41×10^{-6}
4	870.2	863.5	8.42×10^{-3}	4.01×10^{-3}	1.14×10^{-3}	3.74×10^{-4}	1.02×10^{-4}
5	1420	1415	1.95×10^{-2}	4.32×10^{-3}	5.39×10^{-3}	1.21×10^{-2}	3.48×10^{-4}
6	2118	2093	2.302×10^{-2}	2.146×10^{-2}	2.45×10^{-2}	5.34×10^{-2}	2.80×10^{-3}

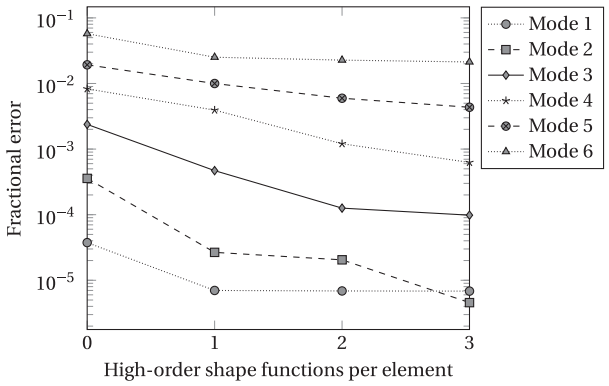

Fig. 7. Error of first six natural frequencies using *h*- and *p*-version FEM, with axial tension of $P = 0.5P_{cr}$.

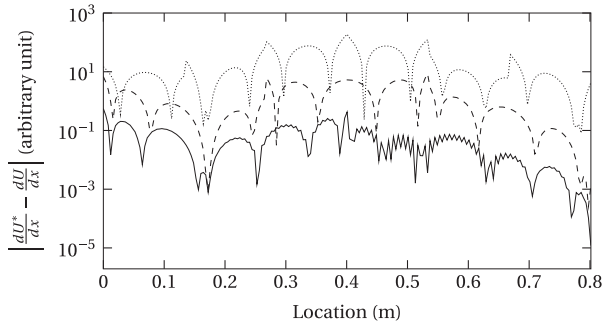

Fig. 8. Bending strain energy error of Timoskenko beam finite elements in Mode 2, with (dotted) $p = 0$, (dashed) $p = 2$ and (solid) $p = 4$.

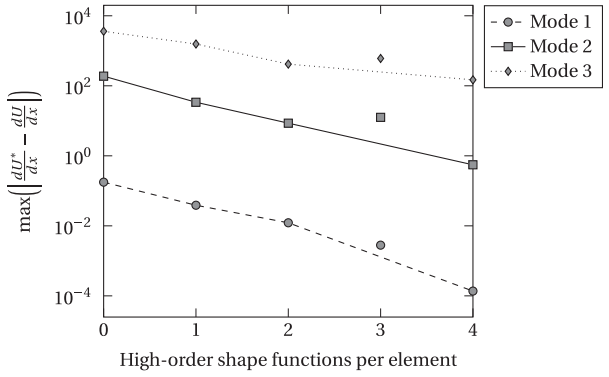

Fig. 9. Bending strain energy error of Timoskenko beam finite elements in various modes. Note: model with $p = 3$ involves 10 DOFs while the others involve 12.

element were compared with those obtained from experiment. Two examples are shown in this section, where one of them corresponds to the rectangular-cross-section beam model demonstrated in the last section, and the another involves an machine tool spindle rotor, whose dimensions are often encountered in practice.

5.1. Cantilever beam

The parameters of the beam (Fig. 13) are identical to those used in static and vibration analysis (Table 2). The "fixed" end is clamped to a workbench. In the modal test, 9 measurement points were taken and the natural frequency was determined using the circle method [8]. In this test, high-order finite element model has 4 elements, with 3 high-order mode shapes per element, which gives a total of 22 DOFs. The natural frequencies obtained in simulations and experiment are listed in Table 5, which shows that the high-order Timoshenko finite element beam model has errors less than 1% on most modes. The large error related to the first mode is due to the flexibility of the clamped end. The mode shapes at the measurement points were compared in terms of the Modal Assurance Criterion (MAC) [8]. The close match of the mode shapes shown in Fig. 14 and the high MAC values between the experimental and numerical modes shows that the high-order Timoshenko beam element is reliable.

5.2. Machine tool spindle rotor

The second experiment was carried out on a machine tool spindle rotor with nominal length of 500 mm. The cross section of the spindle rotor is a hollow circle, with $r_i = 32$ mm and $r_o = 45$–80 mm. The spindle rotor is assumed to be free-free in the FE model and hung with flexible wires in experiment. Due to its geometry, natural frequencies related to bending modes are repeated. 16 measurement points were arranged in two rows along its length, such that both modes in an orthogonal pair could be captured.

Four finite element models were used to predict the natural frequencies and the frequencies were compared with the experimental counterpart. The high-order shape functions are applied to the longer elements. The results are shown in Table 6. As in the first experiment, the discrepancy between the first natural frequencies in models and experimental data is due to the boundary conditions. On other modes which are less affected by the boundary conditions, it can be seen that natural frequencies with high-order Timoshenko finite element model which uses 1-D element are the closest to the experimental counterpart. In addition, such a model uses the least number of DOFs. The results show that the high-order Timoshenko finite element is more accurate than others, together with savings in computation time.

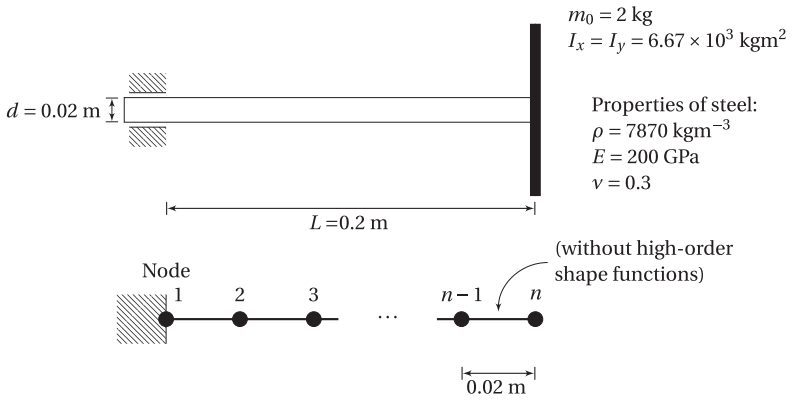

Fig. 10. Layout of rotating shaft model in gyroscopic analysis.

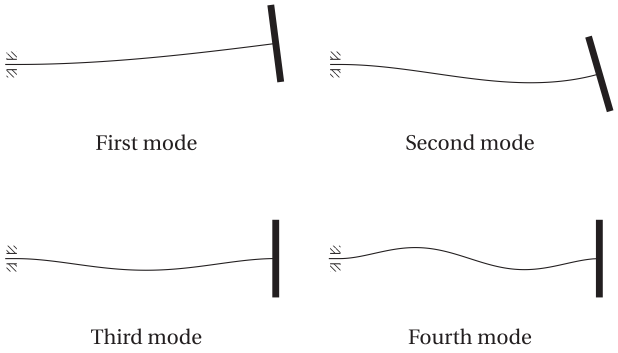

Fig. 11. First four mode shapes of the shaft without rotation.

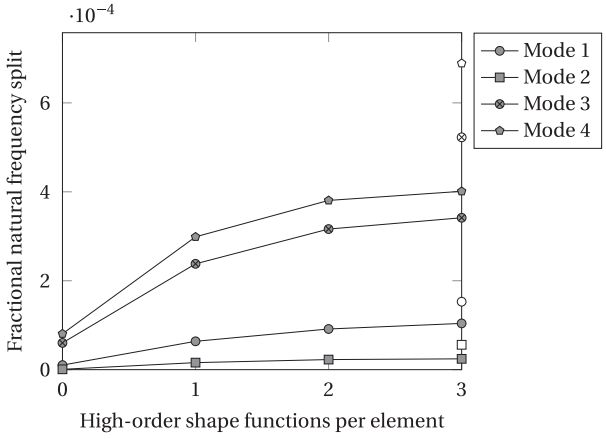

Fig. 12. Extent of fractional natural frequency split at $\Omega_r = 9549$ rpm. The natural frequency split of respective modes in the 200-element model are shown in markers in white.

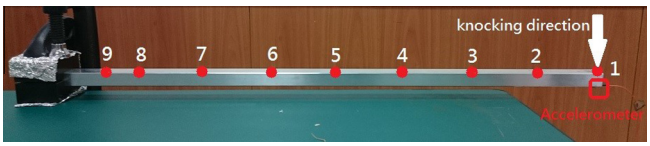

Fig. 13. Cantilever beam tested.

Table 5
Natural frequencies and MAC between beam model and actual cantilever beam.

Mode	Natural frequency (Hz)		Error (%)	MAC
	Experiment	High-order FEM		
1	22.4824	25.4341	13.13	1.000
2	158.416	158.935	0.33	0.998
3	444.126	442.974	−0.26	0.994
4	864.203	862.424	−0.21	0.983
5	1391.338	1414.56	1.67	0.989
6	2074.604	2094.86	0.98	0.983

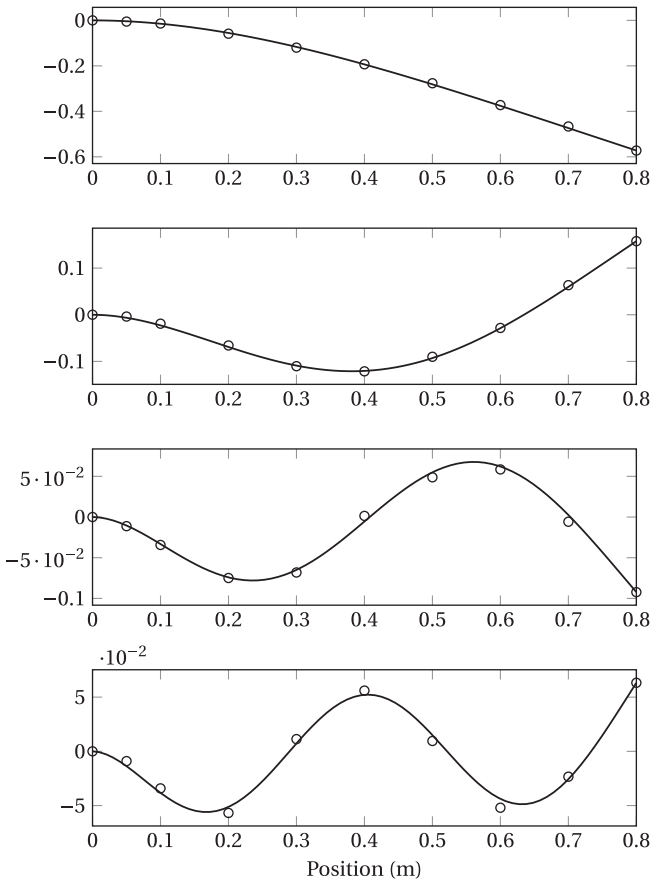

Fig. 14. Mode shapes of cantilever beam from experiment (○) and *p*-version FE model (–).

Table 6
Natural frequencies of spindle rotor.

	EBT	Low-order TBT	High-order TBT (Partial)	ANSYS	Experimental
Elements	30	30	20	39,496	N/A
Mode 1, 2	942.5 Hz	932.7 Hz	932.7 Hz	925.4 Hz	953.9 Hz
Mode 3, 4	2829 Hz	2546 Hz	2544 Hz	2454 Hz	2519 Hz
Mode 5, 6	5941 Hz	4949 Hz	4941 Hz	4721 Hz	4833 Hz

6. Discussion

It is acknowledged that some shape functions and matrix entries involve long expressions as shown in the appendices. However, the error reduction in calculating natural frequencies ω_2 and ω_3, which are often taken for analysis, is significant. The error in the natural frequency split is also reduced. This is an important consideration for algorithms involving repeated calculations, such as in the Monte Carlo simulation and in some optimisation methods. The shape functions can be taken from the appendices directly, or alternatively, interested readers can derive additional shape functions using computer calculations, following the methodology outlined in this article.

7. Conclusions

The shape functions required to perform *p*-type FEM in Timoshenko beams have been established using Legendre polynomials. Correction terms are required in some shape functions to satisfy all constraints. We have also shown that, with a limited number of degree of freedoms, it is beneficial to adopt the *p*-version finite element method to calculate the natural frequencies of beams: the fractional error in the 2nd natural frequencies of a cantilever beam becomes 1/100th of the *h*-version finite element, using the same number of degrees of freedom (DOFs). The model is applied to finding the natural frequencies of real objects and show good agreement with the experimental results.

Acknowledgement

This project is supported by the Ministry of Science and Technology, ROC (Taiwan) Projects MOST102-2218-E-005-006-MY2 and MOST103-2218-E-005-003.

Appendix A. High-order shape functions

Shape functions are given in terms of the isoparametric parameter ξ where

$$\xi = \frac{2x}{L} - 1$$

also

$$\Omega = \frac{EI}{\kappa GAL^2}$$

Rotation shape functions $N_{i\phi}$:

$$[N_\phi] = \frac{1}{1+12\Omega}\begin{Bmatrix} -\frac{3}{2L}(\xi^2-1) \\ \frac{1}{4}\left(3\xi^2 - 2(1+12\Omega)\xi - 1 + 24\Omega\right) \\ \frac{3}{2L}(\xi^2-1) \\ \frac{1}{4}\left(3\xi^2 + 2(1+12\Omega)\xi - 1 + 24\Omega\right) \\ \frac{\sqrt{10}}{8L}\xi(\xi^2-1) \\ \frac{\sqrt{14}}{8L}\left(\frac{5}{4}(\xi^2-1)^2 - \frac{1-\xi^2}{12\Omega+1}\right) \\ \frac{3\sqrt{2}}{32L}\xi(7\xi^2-3)(\xi^2-1) \end{Bmatrix} \tag{A.1}$$

Deflection shape functions N_{iw}:

$$[N_w] = \frac{1}{1+12\Omega}\begin{Bmatrix} \frac{1}{4}\left(\xi^3 - (3+24\Omega)\xi + 2(1+12\Omega)\right) \\ -\frac{L}{8}(-\xi^3 + (1+12\Omega)\xi^2 + \xi - (1+12\Omega)) \\ -\frac{1}{4}\left(\xi^3 - (3+24\Omega)\xi - 2(1+12\Omega)\right) \\ \frac{L}{8}\left(-\xi^3 + (1+12\Omega)\xi^2 - \xi - (1+12\Omega)\right) \\ \frac{\sqrt{10}}{32}\left(\xi^2-1\right)\left(-\xi^2+1+48\Omega\right) \\ -\frac{\sqrt{14}}{64}\xi\left(\xi^2-1\right)\left(\frac{960\Omega^2+108\Omega+1}{(12\Omega+1)} - \xi^2\right) \\ -\frac{\sqrt{2}}{128}\left(\xi^2-1\right)\left(120\Omega\left(1+7\xi^2\right) + 8\xi^2 - 7\xi^4 - 1\right) \end{Bmatrix} \tag{A.2}$$

Appendix B. System matrices for a high-order Timoshenko beam

Stiffness matrix $[K]$:

$$[K] = \frac{EI}{L^3(12\Omega+1)}\begin{bmatrix} 12 & 6L & -12 & 6L & 0 & 0 \\ 6L & 4(3\Omega+1)L^2 & -6L & 2(-6\Omega+1)L^2 & 0 & 0 \\ -12 & -6L & 12 & -6L & 0 & 0 \\ 6L & 2(-6\Omega+1)L^2 & -6L & 4(3\Omega+1)L^2 & 0 & 0 \\ 0 & 0 & 0 & 0 & 2\frac{60\Omega+1}{12\Omega+1} & 0 \\ 0 & 0 & 0 & 0 & 0 & \frac{2(1680\Omega^2+180\Omega+1)}{(12\Omega+1)^2} \end{bmatrix} \tag{B.1}$$

Stiffness matrix due to the axial force $[K_f]$

$$[K_f] = \frac{f_e}{L(12\Omega+1)^2}\begin{bmatrix} k_1 & \frac{L}{10} & -k_1 & \frac{L}{10} & 0 & k_6 \\ \frac{L}{10} & k_2 & -\frac{L}{10} & -k_3 & -k_4 & \frac{k_6}{2L} \\ -k_1 & -\frac{L}{10} & k_1 & -\frac{L}{10} & 0 & -k_6 \\ \frac{L}{10} & -k_3 & -\frac{L}{10} & k_2 & k_4 & \frac{k_6}{2L} \\ 0 & -k_4 & 0 & k_4 & k_5 & 0 \\ k_6 & \frac{k_6}{2L} & -k_6 & \frac{k_6}{2L} & 0 & k_7 \end{bmatrix} \tag{B.2}$$

where

$$k_1 = \frac{6}{5}(120\Omega^2 + 12\Omega + 1),$$

$$k_2 = \frac{2L^2}{15}(90\Omega^2 + 15\Omega + 1),$$

$$k_3 = \frac{L^2}{30}(360\Omega^2 + 60\Omega + 1),$$

$$k_4 = \frac{\sqrt{10L}}{60}(720\Omega^2 + 72\Omega + 1),$$

$$k_5 = \frac{1}{21}(2520\Omega^2 + 84\Omega + 1),$$

$$k_6 = \frac{\sqrt{14}}{70(12\Omega+1)}(1680\Omega^2 + 180\Omega + 1),$$

$$k_7 = \frac{1}{45(12\Omega+1)^2}(1814400\Omega^4 + 388800\Omega^3 + 23040\Omega^2 + 240\Omega + 1).$$

The Mass matrix $[M]$ is the sum of the "translation" term $[M_w]$ and the "rotation" term $[M_\phi]$:

$$[M] = \frac{\rho AL}{(12\Omega+1)^2}[M_w] + \frac{\rho I}{(12\Omega+1)^2}[M_\phi]$$

where

$$[M_w]=\begin{bmatrix} \frac{1680\Omega^2+294\Omega+13}{35} & L\frac{1260\Omega^2+231\Omega+11}{210} & \frac{3(560\Omega^2+84\Omega+3)}{70} & -L\frac{2520\Omega^2+378\Omega+13}{420} & m_{w51} & m_{w61} \\ & L^2\frac{126\Omega^2+21\Omega+1}{105} & L\frac{2520\Omega^2+378\Omega+13}{420} & -L^2\frac{168\Omega^2+28\Omega+1}{140} & -m_{w52} & m_{w62} \\ & & \frac{1680\Omega^2+294\Omega+13}{35} & -L\frac{1260\Omega^2+231\Omega+11}{210} & m_{w51} & -m_{w61} \\ & & & L^2\frac{126\Omega^2+21\Omega+1}{105} & m_{w52} & m_{w62} \\ & & & & m_{w55} & 0 \\ \text{sym.} & & & & & m_{w66} \end{bmatrix} \tag{B.3}$$

$$[M_\phi]=\begin{bmatrix} \frac{6}{5L} & -\frac{1}{10}(60\Omega-1) & -\frac{6}{5L} & -\frac{1}{10}(60\Omega-1) & 0 & -m_{\phi61} \\ & \frac{2L}{15}(360\Omega^2+15\Omega+1) & \frac{1}{10}(60\Omega-1) & \frac{L}{30}(720\Omega^2-60\Omega-1) & m_{\phi52} & m_{\phi62} \\ & & \frac{6}{5L} & \frac{1}{10}(60\Omega-1) & 0 & m_{\phi61} \\ & & & \frac{2L}{15}(360\Omega^2+15\Omega+1) & -m_{\phi52} & m_{\phi62} \\ & & & & \frac{1}{21L} & 0 \\ \text{sym.} & & & & & m_{\phi66} \end{bmatrix} \tag{B.4}$$

where

$$m_{w51}=-\frac{\sqrt{10}}{120}(720\Omega^2+72\Omega+1),$$
$$m_{w52}=\frac{\sqrt{10}}{560}(672\Omega^2+68\Omega+1),$$
$$m_{w55}=\frac{1}{252}(3024\Omega^2+108\Omega+1),$$
$$m_{w61}=\frac{\sqrt{14}}{630(12\Omega+1)}(15120\Omega^3+3240\Omega^2+183\Omega+1),$$
$$m_{w62}=\frac{\sqrt{14}L}{5040(12\Omega+1)}(1440\Omega^2+156\Omega+1)),$$
$$m_{w66}=\frac{1}{1980(12\Omega+1)^2}(1900800\Omega^4+411840\Omega^3+24960\Omega^2+288\Omega+1),$$

and

$$m_{\phi52}=\frac{\sqrt{10}}{60}(12\Omega+1) \qquad m_{\phi61}=\frac{\sqrt{14}(180\Omega+1)}{70L(12\Omega+1)},$$
$$m_{\phi62}=\frac{\sqrt{14}(1680\Omega^2-40\Omega-1)}{140(12\Omega+1)} \qquad m_{\phi66}=\frac{(3600\Omega^2+60\Omega+1)}{45L(12\Omega+1)^2}.$$

Gyroscopic matrix $[G]$:

$$[G]=\frac{\rho I}{5L(12\Omega+1)^2}\begin{bmatrix} 0 & 12 & g_2 & 0 & 0 & -12 & g_2 & 0 & 0 & 0 & 0 & -g_7 \\ -12 & 0 & 0 & g_2 & 12 & 0 & 0 & g_2 & 0 & 0 & g_7 & 0 \\ -g_2 & 0 & 0 & g_3 & g_2 & 0 & 0 & -g_4 & g_5 & 0 & -g_8 & 0 \\ 0 & -g_2 & -g_3 & 0 & 0 & g_2 & g_4 & 0 & 0 & g_5 & 0 & -g_8 \\ 0 & -12 & -g_2 & 0 & 0 & 12 & -g_2 & 0 & 0 & 0 & 0 & g_7 \\ 12 & 0 & 0 & -g_2 & -12 & 0 & 0 & -g_2 & 0 & 0 & -g_7 & 0 \\ -g_2 & 0 & 0 & -g_4 & g_2 & 0 & 0 & g_3 & -g_5 & 0 & -g_8 & 0 \\ 0 & -g_2 & g_4 & 0 & 0 & g_2 & -g_3 & 0 & 0 & -g_5 & 0 & -g_8 \\ 0 & 0 & -g_5 & 0 & 0 & 0 & g_5 & 0 & 0 & \frac{2}{105} & 0 & 0 \\ 0 & 0 & 0 & -g_5 & 0 & 0 & 0 & g_5 & -\frac{2}{105} & 0 & 0 & 0 \\ 0 & -g_7 & g_8 & 0 & 0 & g_7 & g_8 & 0 & 0 & 0 & 0 & g_9 \\ g_7 & 0 & 0 & g_8 & -g_7 & 0 & 0 & g_8 & 0 & 0 & -g_9 & 0 \end{bmatrix} \tag{B.5}$$

where

$$g_2=L(60\Omega-1),$$
$$g_3=4/3L^2(360\Omega^2+15\Omega+1),$$
$$g_4=1/3L^2(-720\Omega^2+60\Omega+1),$$
$$g_5=\sqrt{106}L(12\Omega+1),$$
$$g_7=\frac{\sqrt{14}}{7(12\Omega+1)}(180\Omega+1),$$
$$g_8=\frac{\sqrt{14}L}{14(12\Omega+1)}(-1680\Omega^2+16\Omega+1),$$
$$g_9=\frac{2}{9(12\Omega+1)^2}(3600\Omega^2+60\Omega+1).$$

References

[1] Babuska I, Szabo B, Katz I. The p-version of the finite element method. SIAM J Numer Anal 1981;18(3):515–45.
[2] Bhaskar A. Elastic waves in Timoshenko beams: the 'lost and found' of an eigenmode. Proc R Soc A: Math Phys Eng Sci 2009;465(2101):239–55.
[3] Chan Y-J, Ewins DJ. A comprehensive procedure to estimate the probability of extreme vibration levels due to mistuning. J Eng Gas Turbines Power 2010;132(11):112505.
[4] Cowper GR. The shear coefficient in Timoshenko's beam theory. J Appl Mech 1966;33(2):335–40.
[5] de Anda AD, Flores J, Gutiérrez L, Médez-Sánchez R, Monsivais G, Morales A. Experimental study of the Timoshenko beam theory predictions. J Sound Vib 2012;331(2–6):5732–44.
[6] Düster A, Bröker H, Rank E. The p-version of the finite element method for three-dimensional curved thin walled structures. Int J Numer Meth Eng 2001;52(7):673–703.
[7] Ertürk A, Özgüven H, Budak E. Analytical modeling of spindle–tool dynamics on machine tools using Timoshenko beam model and receptance coupling for the prediction of tool point FRF. Int J Mach Tools Manuf 2006;46(15):1901–12.
[8] Ewins DJ. In: Modal testing: theory, practice and application. Research Studies Press; 2000.
[9] Friedman Z, Kosmatka J. An improved two-node Timoshenko beam finite element. Comput Struct 1993;47(3):473–81.
[10] Friswell M, Penny J, Garvey S, Lees A. Dynamics of rotating machines. Cambridge University Press; 2010.
[11] Gruttmann F, Wagner W. Shear correction factors in Timoshenko's beam theory for arbitrary shaped cross-sections. Comput Mech 2001;27:199–207.
[12] Han SM, Benaroya H, Wei T. Dynamics of transversely vibrating beams using four engineering theories. J Sound Vib 1999;225(5):935–88.
[13] Horr AM, Schmidt LC. Closed-form solution for the Timoshenko beam theory using a computer-based mathematical package. Comput Struct 1995;55:405–12.
[14] Hutchinson JR. Shear coefficients for Timoshenko beam theory. J Appl Mech Trans ASME 2001;68:87–92.
[15] Kosmatka JB. An improved two-node finite element for stablility and natural frequencies of axial-load Timoshenko beams. Comput Struct 1995;57:141–9.
[16] Majkut L. Free and forced vibrations of Timoshenko beams described by single difference equation. J Theor Appl Mech 2009;47(1):193–210.
[17] Meirovitch L, Baruh H. On the inclusion principle for the hierarchical finite element method. Int J Numer Meth Eng 1983;19(2):281–91.

[18] Nesterenko V. A theory for transverse vibration of the Timoshenko beam. J Appl Math Mech 1993;57(4):669–77.
[19] Oñate E. Structural analysis with the finite element method. Linear statics: volume 2: beams, plates and shells. In: Lecture notes on numerical methods in engineering and sciences. International Center for Numerical Methods in Engineering (CIMNE); 2013 [chapter 2].
[20] Petyt M. Introduction to finite element vibration analysis. 2nd ed. Cambridge; 2010.
[21] Reddy J. On locking-free shear deformable beam finite elements. Comput Methods Appl Mech Eng 1997;149:113–32.
[22] Reddy J. On the dynamic behaviour of the Timoshenko beam finite elements. Sadhana 1999;24(3):175–98.
[23] Rosinger HE, Ritchie IG. On Timoshenko's correction for shear in vibrating isotropic beams. J Phys D: Appl Phys 1977;10(11):1461.
[24] Stephen N. The second spectrum of Timoshenko beam theory–further assessment. J Sound Vib 2006;292(1–2):372–89.
[25] Stephen N, Puchegger S. The second frequency spectrum of Timoshenko beams. J Sound Vib 1982;80:578–82.
[26] Timoshenko S. On the transverse vibrations of bars of uniform cross-section. Phil Mag 1922;43:125–31.
[27] Zienkiewicz O, Taylor R, Fox D. The finite element method for solid and structural mechanics. 7th ed. Butterworth-Heinemann; 2013.